PHYSICAL REVIEW E **93**, 010901(R) (2016)

Extreme stiffness tunability through the excitation of nonlinear defect modes

M. Serra-Garcia,[1,*] J. Lydon,[1] and C. Daraio[1,2]

[1]*Department of Mechanical and Process Engineering, Swiss Federal Institute of Technology (ETH), Zurich 8092, Switzerland*

[2]*Engineering and Applied Science, California Institute of Technology, Pasadena, California 91125, USA*

(Received 2 February 2015; revised manuscript received 7 December 2015; published 12 January 2016)

The incremental stiffness characterizes the variation of a material's force response to a small deformation change. In lattices with noninteracting vibrational modes, the excitation of localized states does not have any effect on material properties, such as the incremental stiffness. We report that, in nonlinear lattices, driving a defect mode introduces changes in the static force-displacement relation of the material. By varying the defect excitation frequency and amplitude, the incremental stiffness can be tuned continuously to arbitrarily large positive or negative values. Furthermore, the defect excitation parameters also determine the displacement region at which the force-displacement relation is being tuned. We demonstrate this phenomenon experimentally in a compressed array of spheres tuning its incremental stiffness from a finite positive value to zero and continuously down to negative infinity.

DOI: 10.1103/PhysRevE.93.010901

Defects are ubiquitous in materials. Initially thought to decrease a material's performance, deliberately introducing defects is now key to achieving desirable properties [1]. A characteristic feature of defects is that they allow localized states of vibration to exist in the vicinity of a defect [2]. Previous studies have explored the effect of these defect modes on the electrical [3], thermal [4,5], and optomechanical [6] properties of materials. Here we attempt the deliberate excitation of localized defect resonances as a means to change bulk material properties. Having materials with extreme properties is desirable from a practical point of view because they enable devices that can focus [7], cloak [8–10], or mitigate vibrations [11] with a performance greater than that allowed by conventional wave mechanics. This desire has motivated the use of resonances [9,11], buckling elements [12], negative stiffness inclusions [13,14], or magnetic coupling between particles [15,16] in order to achieve a stiffness that is negative, zero, or higher than that of diamond. These principles result in extreme material properties but only over a narrow range of displacements [12], frequencies [17], or temperatures [13,18].

In this Rapid Communication, we demonstrate a physical mechanism that results in extreme values of the incremental stiffness, defined as the change in the material's reaction force when its deformation is changed. The mechanism is based on the nonlinear interaction between lattice particles. A distinctive property of nonlinear lattices is the presence of thermal expansion [19] in which the lattice expands or contracts as a response to an increase or decrease in its vibrational energy. In our system, we drive a defect mode in a lattice with a harmonic signal. As a consequence of anharmonicity in the lattice, an external deformation affects the resonance frequency of the defect. This causes the defect mode to move in and out of resonance when the lattice is deformed. The resulting changes in the vibrational amplitude cause a dynamic expansion or contraction of the defect. This affects the force at the boundary and therefore alters the incremental stiffness of the lattice. We use this concept to achieve negative stiffness [Fig. 1(a)].

We demonstrate the concept experimentally in a one-dimensional lattice of nine coupled steel (Young modulus $E = 210$ GPa [20]) spheres. The spheres have a radius of 9.525 mm and a mass of $28.4g$, except for two particles in the center [see Fig. 1(a) and the Supplemental Material [21]). The interaction between the spheres is modeled using the Hertzian contact law [22]. The central particle is a defect that allows the existence of a localized vibrational mode [2,22,23]. The defect is a 4.763-mm sphere. The particle next to the defect consists of a piezoelectric actuator sandwiched between two steel cylinders with $r = 20$ and $h = 4$ mm. This particle is used to harmonically excite the defect mode. The lattice is kept in place using two polycarbonate rods. We monitor the defect mode vibration using a laser Doppler vibrometer pointing at the particle next to the defect. We acquire the quasistatic force-displacement relation of the lattice by prescribing an external deformation using a piezoelectric actuator placed at one end of the chain while simultaneously measuring the force at the opposite boundary. The vibration of the defect mode affects the force-displacement relation. The amplitude and frequency of the defect excitation control the mechanical properties of the material. Using these variables we can select both the incremental stiffness magnitude (Fig. 1(b) and the Supplemental Material [21]) and the displacement point where the incremental stiffness is being modified (Fig. 1(c) and the Supplemental Material [21]). This allows tuning the force-displacement response of a lattice at a selectable displacement value, a capability that exists in biological organisms [24] but not in systems that exhibit negative stiffness when subject to an external energy input [25,26].

Due to the nonlinearity of the lattice, the measured force depends on both the applied displacement and the amplitude of the mode $F(X,A)$. Therefore, the incremental stiffness, defined as the total derivative of the force with respect to the displacement, is given by the equation,

$$\frac{dF}{dx} = \left(\frac{\partial F}{\partial X}\right)_A + \left(\frac{\partial F}{\partial A}\right)_X \frac{\partial A}{\partial X}. \tag{1}$$

The first term on the right side of Eq. (1) gives the stiffness of the lattice neglecting any change in the defect

*sermarc@ethz.ch

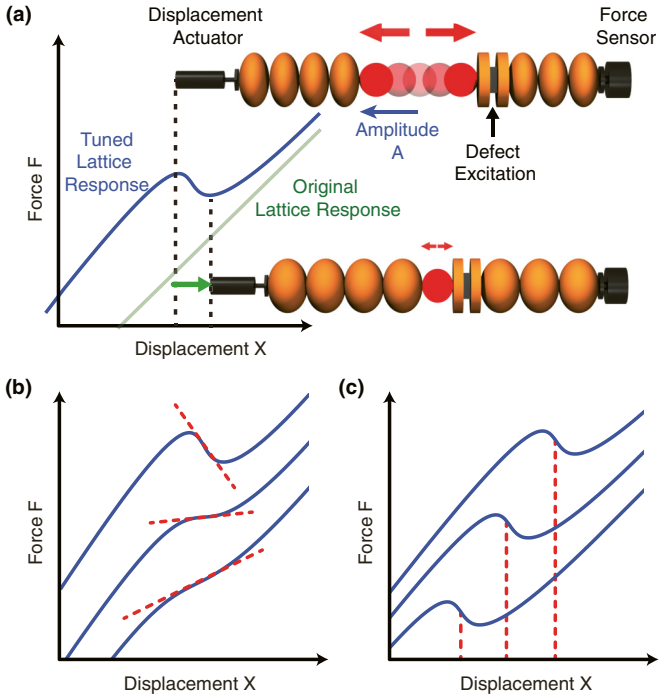

FIG. 1. Tuning the stiffness through dynamic expansion. (a) Schematic of the tunable stiffness mechanism illustrated in a one-dimensional granular chain. The diagram shows the response of the lattice to a prescribed boundary displacement. During this displacement the defect is subject to a harmonic excitation at a fixed frequency and amplitude, as a consequence, it vibrates with an amplitude A. As the lattice is compressed (green arrow), the defect mode is detuned from the excitation signal (red arrows). This results in a negative incremental stiffness due to dynamic contraction of the defect mode. (b) Changes in the driving frequency and amplitude of the excitation determine the incremental stiffness, and (c) the strain point at which the stiffness is being modified. The curves are offset for clarity.

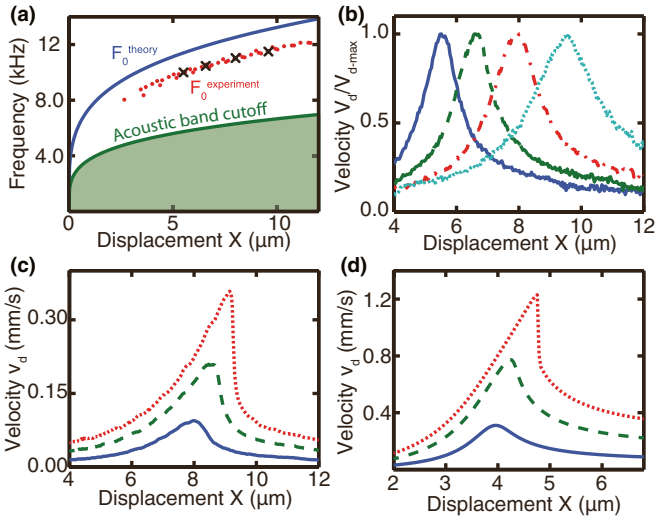

FIG. 2. Response of the nonlinear defect mode. (a) Theoretical defect mode (blue) and acoustic band (green) frequencies dependence on the prescribed displacement. Experimental measurements are plotted as red dots with the four curves in panel (b) marked with black crosses. (b) Normalized experimental velocity of the defect mode as a function of displacement of the lattice. Curves correspond to excitation frequencies of 10 (blue, solid line), 10.5 (green, dashed line), 11 (red, dashed-dotted line), and 11.5 kHz (cyan, dotted line). The frequencies in panel (a) are obtained by fitting these curves using a Lorentzian function. (c) Experimental velocity of the defect mode v_d, measured at the site next to the defect particle for drive amplitudes of 4.2 (blue, solid line), 9.8 (green, dashed line), and 15.4 nm (red, dotted line) all at 10.5 kHz. (d) Numerical results corresponding to (c) for defects driven at 20, 50, and 80 nm, respectively. Our discrete particle model (see the Supplemental Material [21]) qualitatively reproduces the experimental results but is unable to make precise quantitative predictions, and this could be due to the fact that our model neglects experimental factors, such as internal particle and actuator resonances, as well as the nonlinear friction between the particles and the rods.

mode's amplitude. The second term describes the effect of the oscillation of the defect mode. The function $(\partial F/\partial A)_X$ is the change in the force due to a change in amplitude of the defect mode and quantifies the intensity of the thermal expansion. From a dynamical point of view, this arises due to an asymmetry of the interaction potential [19] and in our lattice is always positive (see the Supplemental Material [21]). Finally, the effect of the strain on the amplitude of the mode is contained in the quantity $\partial A/\partial X$.

The vibration amplitude's dependence on strain is a consequence of the harmonic excitation and of the nonlinearity present in the chain. The harmonic excitation results in a defect mode resonance, which occurs when the defect mode's frequency F_0 matches the excitation frequency F_d. The nonlinearity relates the mode's frequency F_0 to the lattice strain X [22]. In our system the Hertzian contact results in the relationship $F_0 \propto X^{1/4}$. As a result, straining the lattice causes a change in the mode's frequency [Fig. 2(a)]. If the mode's frequency approaches the excitation frequency, the mode gets closer to resonance, and therefore the oscillation amplitude increases. Conversely, if the mode frequency moves away from the excitation frequency, the oscillation amplitude decreases [Fig. 2(b)]. This strain controlled resonance results in a dependence of amplitude on strain and therefore, in a nonzero $\partial A/\partial x$.

Different excitation frequencies cause the resonance to happen at different strain values [Figs. 2(a) and 2(b)]. This is due to the aforementioned frequency strain relationship, which associates a particular resonance strain with each excitation frequency. By choosing the excitation frequency we are able to set the displacement region where the system is in resonance and the stiffness is being modified [Fig. 2(b)].

The effect of the excitation amplitude on the defect's vibration is shown in Figs. 2(c) and 2(d). As expected, driving the defect with larger harmonic forces results in larger oscillations. Furthermore, as the excitation amplitude gets larger the resonance response becomes increasingly asymmetric. This is a common property of driven nonlinear oscillators close to a bifurcation [27]. As the nonlinear systems approach the bifurcation points, oscillations become extremely sensitive to the strain [28]; in our system the magnitude of

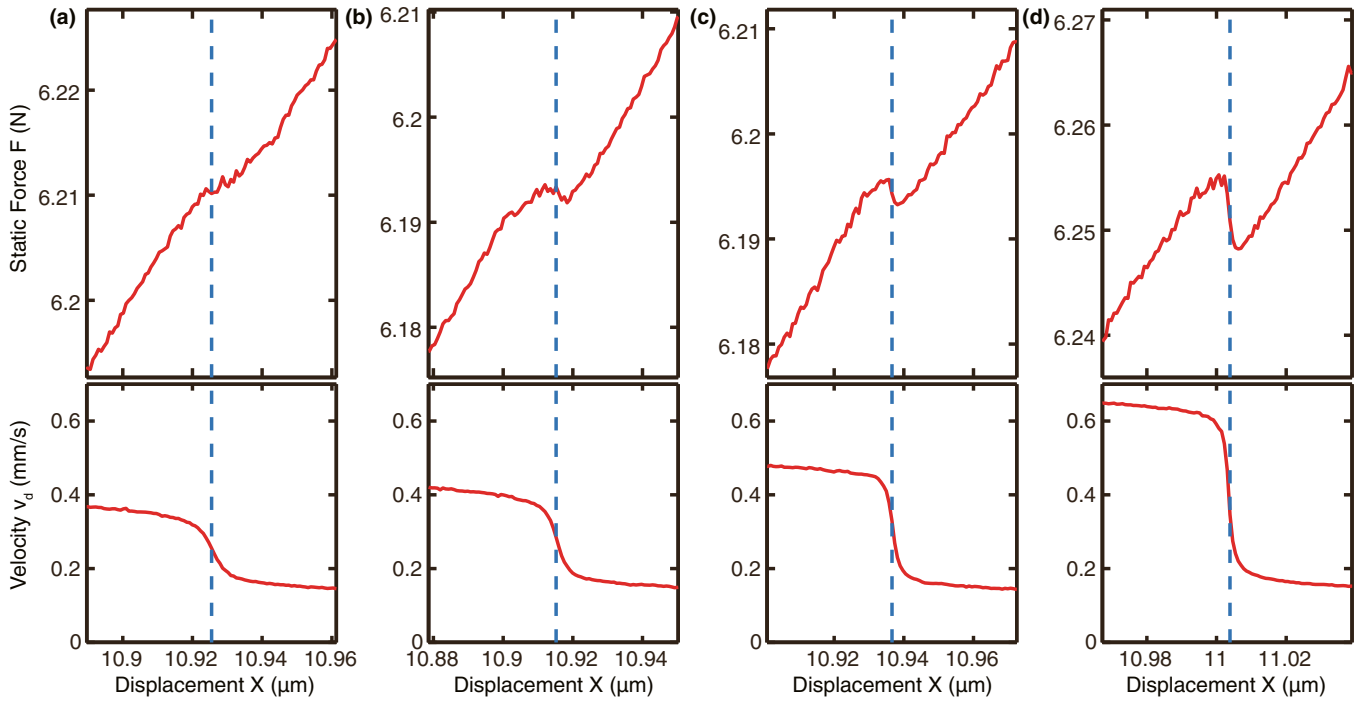

FIG. 3. Experimental tuning of the incremental stiffness. Force-displacement curves for excitation amplitudes of (a) 5.9 nm, (b) 6.4 nm, (c) 7.54 nm, and (d) 10.9 nm. Shown below are the defect mode velocities [proportional to the mode amplitude $A(x)$] as a function of the overall displacement x of the lattice. In panel (d), the system discontinuously transitions between two oscillation branches. This introduces a region of completely vertical slope in the force-displacement curve. The curves have been measured at an increasing displacement rate of 0.53 nm s.

$\partial A/\partial x$ approaches minus infinity. This allows us to achieve arbitrarily large negative values of incremental stiffness.

These extreme negative values have been attained experimentally. The measured force-displacement curves at four different drive amplitudes are shown in Fig. 3. The incremental stiffness at our selected strain progressively decreases as the defect excitation is increased [Figs. 3(a)–3(d)]. For the largest excitation amplitude, the force-displacement curve is discontinuous, indicating that the stiffness is extremely negative [Fig. 3(d)]. This indicates that the excitation is very close or above the bifurcation amplitude. In order to validate that this effect is due to the defect's vibration, we simultaneously measure the defect's mode amplitude, presented below each force-displacement curve in Figs. 3(a)–3(d). The greatest change in the incremental stiffness happens where the slope $\partial A/\partial x$ is the most negative. This occurs because larger changes in vibrational amplitude are accompanied by larger changes in dynamic expansion. The forces introduced by this dynamic expansion are small, a feature that we attribute to the dimensions of our system and the properties of the Hertzian interaction. It should be noted that the negative stiffness values are stable because our experiment is performed under prescribed displacement boundary conditions.

Each pair of drive frequency and amplitude results in a determined incremental stiffness at a particular displacement point. We explore this relationship analytically by constructing a discrete particle model. The model accounts for the nonlinear interaction between particles and for losses due to linear damping. (see the Supplemental Material for a complete description [21]) in Fig. 4(a). The blue lines show contours at the same excitation amplitude, and the red lines show contours at the same frequency. To get a particular stiffness at a desired displacement, we select the excitation parameters corresponding to the lines passing through this point. Although we only show a finite number of constant lines, all possible values in the shaded region are attainable. In the theoretical model, the stiffness tuning mechanism works for arbitrarily large displacements; in practice, the system will be limited to a smaller range due to the presence of plastic deformation at the contacts.

A remarkable feature of the mechanism presented in this Rapid Communication is that it results in a zero incremental stiffness for certain defect excitation parameters. In this region the material will support a load, but it will not transmit any vibration to it, which is of great practical relevance [29]. In the zero stiffness region the lattice will have a zero frequency band gap. Tunable band gaps in mechanical metamaterials can be found in the literature [30,31]. However, a distinctive feature of our mechanism is that it leads to band gaps centered at zero frequency. We simulate the band gap using our numerical model. In the simulation, the lattice is subject to a static compression. We adjust the defect's excitation frequency and amplitude to tune the stiffness to zero at this compression value. We then apply a very small amplitude periodic deformation at one end of the chain. The deformation has a frequency f_L. Simultaneously, we monitor the transmitted force at the other end [Fig. 4(b)]. We can see that the band gap exists only at low frequencies and that that high frequency deformations can propagate without attenuation. We quantify the width of the band gap by fitting the transmission to a first order high pass filter $H(f_L) = (f_L/f_c)/\sqrt{1+(f_L/f_c)^2}$. This results in

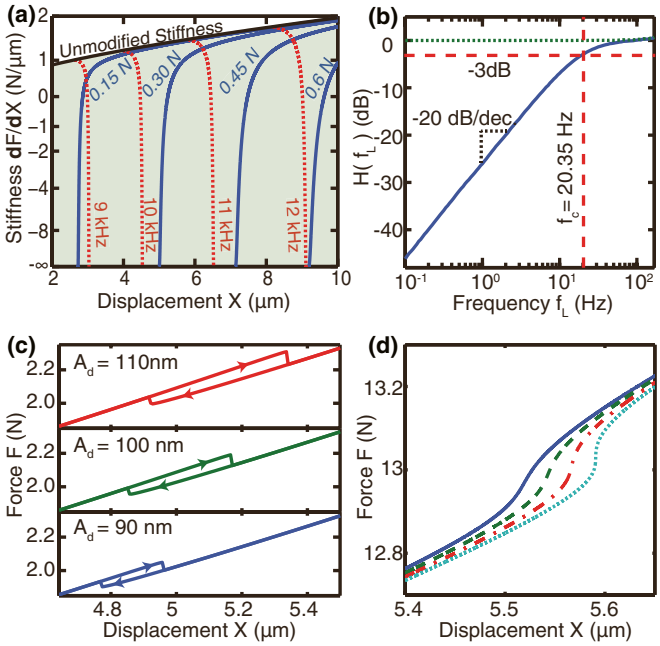

FIG. 4. Theoretical investigation. (a) Map relating the excitation parameters with the modified incremental stiffness and displacement point. Each point position on the map corresponds to tuning the stiffness to the value on the Y axis at the displacement point indicated by the X axis. Each dotted red line defines a set of tuned stiffness states that are accomplished by the same excitation frequency. The solid blue lines represent sets of tuned stiffness that are attained by the same excitation amplitude. The intersection between red lines and blue lines determines the excitation frequency and amplitude required to achieve the stiffness labeled by the Y axis at the displacement labeled by the X axis. (b) Zero frequency band gap obtained by choosing excitation parameters corresponding to zero stiffness for the lattice. The blue and green lines show the force transmitted with the defect drive on and off, respectively. When the defect excitation is turned off, the lattice acts as a linear spring for small deformations around the prescribed displacement value; when the defect excitation is turned on, there is a band gap centered at zero frequency. The dotted red line shows the band gap edge frequency f_c. (c) Force-displacement relationships of the system when it is driven above the bifurcation amplitude. The presence of a tunable hysteresis allows the system to be used as a tunable damper. (d) Analytical force-displacement relation for a lattice of particles with the nonlinear interaction force law $F(\delta) = A\delta^{0.5}$ (see the Supplemental Material for details on the parameters used [21]) with a defect excitation frequency of 13.5 KHz and amplitudes 0.72 N (blue, solid line), 0.74 N (green, dashed line), 0.76 N (red, dashed-dotted line), and 0.78 N (cyan, dotted line). For this potential exciting the defect mode results in an arbitrarily large positive stiffness.

a cutoff frequency of $f_c = 20.35$ Hz. The upper end of the band gap is a consequence of the fact that the predicted zero stiffness force versus the displacement relationship assumes a defect mode oscillating in a steady state. When we change the deformation of the lattice, the steady-state oscillation of the defect is perturbed. The system cannot recover the steady-state motion instantaneously. The time it takes for the defect mode to relax back to its steady state limits the upper frequency of the band gap. The speed of the system can be analyzed by using a linear perturbation method (for the Floquet analysis, see the Supplemental Material [21]). It is possible to attain higher cutoff frequencies by using smaller particles (see the Supplemental Material of Ref. [22]).

At the point where the stiffness reaches minus infinity, the dynamics undergoes a bifurcation. Bifurcations are known to occur in granular lattices with defects [32]. At this bifurcation point the system goes from having a single solution to having multiple stable solutions [27]. This leads to a hysteretic force-displacement response with the system following different paths when contracting or expanding [Fig. 4(c)]. The area of the hysteresis loop corresponds to the loss of energy incurred as the lattice is driven around a compression cycle. The nonconservative forces in the system, represented by the damping and the defect excitation, will dissipate the lost energy and return the system to its initial state after a cyclic deformation. Since changing the drive amplitude can control the area enclosed in the hysteresis loop, this effect can be used to implement tunable dampers. We present an experimental observation of the tunable damping in the Supplemental Material [21].

The changes in the stiffness that we present in this Rapid Communication arise due to the presence of a strain-controlled resonance and due to thermal expansion. These effects are a consequence of the nonlinear interaction between the lattice particles. The nonlinear interaction potential determines the sign of the thermal expansion as well as the shape and strain dependence of the defect resonance. Therefore, the interparticle interaction potential determines whether the lattice's stiffness will become extremely positive or extremely negative when driving the defect mode. We explore the effect of different interaction potentials in the Supplemental Material [21]. For the case of a force law of the form $F(\delta) = A\delta^{0.5}$ the excitation of the defect mode results in an increase in the stiffness, that can reach arbitrarily high values. Figure 4(d) presents the analytical force-displacement curves for this case.

We have investigated the stiffness of a lattice subject to localized defect state excitations. The nonlinearity couples the motion of the defect mode to the bulk properties of the lattice. This results in a stiffness that can take arbitrarily large positive, zero, or negative values. This effect can introduce zero frequency band gaps, and for high excitation forces, the system becomes hysteretic and can act as a tunable damper. Future studies should elucidate the equivalent phenomenon in two-dimensional and three-dimensional lattices and explore the effect of engineered interaction potentials in the speed and performance of the system. Although our study has focused on the effect of localized excitations on mechanical properties, we expect an analogous phenomenon to exist in electromagnetic systems, such as varactor loaded split ring resonator arrays (VLSRR). This is due to the fact that those systems present quadratic [33] and cubic [34] nonlinearities as well as a dependence of resonances on an external static bias [35].

We acknowledge support from the U.S.-AFOSR (Grant No. FA9550-12-1-0332) and the Army Research Office MURI U.S. ARO (Grant No. W911NF-09-1-0436).

[1] H. J. Queisser and E. E. Haller, Science **281**, 945 (1998).
[2] E. W. Montroll and R. B. Potts, Phys. Rev. **100**, 525 (1955).
[3] J.-H. Chen, C. Jang, S. Xiao, M. Ishigami, and M. S. Fuhrer, Nat. Nanotechnol. **3**, 206 (2008).
[4] A. A. Balandin, Nature Mater. **10**, 569 (2011).
[5] M. Wagner, Phys. Rev. **131**, 1443 (1963).
[6] E. Gavartin, R. Braive, I. Sagnes, O. Arcizet, A. Beveratos, T. J. Kippenberg, and I. Robert-Philip, Phys. Rev. Lett. **106**, 203902 (2011).
[7] J. B. Pendry, Phys. Rev. Lett. **85**, 3966 (2000).
[8] X. Zhu, B. Liang, W. Kan, X. Zou, and J. Cheng, Phys. Rev. Lett. **106**, 014301 (2011).
[9] W. M. Graeme, New J. Phys. **9**, 359 (2007).
[10] S. Zhang, C. Xia, and N. Fang, Phys. Rev. Lett. **106**, 024301 (2011).
[11] Z. Liu, X. Zhang, Y. Mao, Y. Y. Zhu, Z. Yang, C. T. Chan, and P. Sheng, Science **289**, 1734 (2000).
[12] B. Florijn, C. Coulais, and M. van Hecke, Phys. Rev. Lett. **113**, 175503 (2014).
[13] T. Jaglinski, D. Kochmann, D. Stone, and R. S. Lakes, Science **315**, 620 (2007).
[14] C. S. Wojnar and D. M. Kochmann, Philos. Mag. **94**, 532 (2013).
[15] M. Lapine, I. V. Shadrivov, D. A. Powell, and Y. S. Kivshar, Nat. Mater. **11**, 30 (2012).
[16] C. Majidi and R. J. Wood, Appl. Phys. Lett. **97**, 164104 (2010).
[17] N. Fang, D. Xi, J. Xu, M. Ambati, W. Srituravanich, C. Sun, and X. Zhang, Nat. Mater. **5**, 452 (2006).
[18] L. Dong, D. S. Stone, and R. S. Lakes, Phys. Status Solidi B **245**, 2422 (2008).
[19] C. Kittel, *Introduction to Solid State Physics* (Wiley, Hoboken, NJ, 1996).
[20] *ASM International*, Metals Handbook 10th ed. (ASM International, Materials Park, OH, 1990).
[21] See Supplemental Material at http://link.aps.org/supplemental/10.1103/PhysRevE.93.010901 for details on numerical and experimental methods, analytical approximations, and the transient response of the system, and for animations depicting selective force-displacement relationship tunability.
[22] Y. Man, N. Boechler, G. Theocharis, P. G. Kevrekidis, and C. Daraio, Phys. Rev. E **85**, 037601 (2012).
[23] N. Boechler, G. Theocharis, and C. Daraio, Nat. Mater. **10**, 665 (2011).
[24] P. Martin, A. D. Mehta, and A. J. Hudspeth, Proc. Natl. Acad. Sci. USA **97**, 12026 (2000).
[25] J. M. T. Thompson, Nature (London) **296**, 135 (1982).
[26] R. Lakes, Philos. Mag. Lett. **92**, 226 (2012).
[27] A. H. Nayfeh and D. T. Mook, *Nonlinear Oscillations* (Wiley, Hoboken, NJ, 2008).
[28] R. B. Karabalin, R. Lifshitz, M. C. Cross, M. H. Matheny, S. C. Masmanidis, and M. L. Roukes, Phys. Rev. Lett. **106**, 094102 (2011).
[29] R. A. Ibrahim, J. Sound Vib. **314**, 371 (2008).
[30] N. Boechler, J. Yang, G. Theocharis, P. G. Kevrekidis, and C. Daraio, J. Appl. Phys. **109**, 074906 (2011).
[31] P. Wang, F. Casadei, S. Shan, J. C. Weaver, and K. Bertoldi, Phys. Rev. Lett. **113**, 014301 (2014).
[32] G. Theocharis, M. Kavousanakis, P. G. Kevrekidis, C. Daraio, M. A. Porter, and I. G. Kevrekidis, Phys. Rev. E **80**, 066601 (2009).
[33] S. Larouche, A. Rose, E. Poutrina, D. Huang, and D. R. Smith, Appl. Phys. Lett. **97**, 011109 (2010).
[34] D. Huang, E. Poutrina, and D. R. Smith, Appl. Phys. Lett. **96**, 104104 (2010).
[35] M. Maasch, C. Damm, M. Schüssler, E. González-Rodríguez, and R. Jakoby, *German Microwave Conference (GeMIC)* (IEEE, 2011).